# Comparison of the Responsivity of Solution-Suspended and Surface-Bound Poly (*N*-isopropylacrylamide)-Based Microgels for Sensing Applications

Wenxiang Li,[1] Liang Hu,[*,1,2] Jinghua Zhu,[2,3] Dan Li,[4] Yafei Luan,[4] Wenwen Xu[2] and Michael J. Serpe[*,2]

1. School for Radiological and Interdisciplinary Sciences (RAD-X), Collaborative Innovation Center of Radiation Medicine of Jiangsu Higher Education Institutions and Jiangsu Provincial Key Laboratory of Radiation Medicine and Protection, Soochow University, Suzhou, Jiangsu, 215123, China

2. Department of Chemistry, University of Alberta, Edmonton, AB, T6G 2G2, Canada

3. The Institute of Petrochemistry, Heilongjiang Academy of Sciences, Harbin, Heilongjiang, 150040, China

4. College of Chemistry, Chemical Engineering and Materials Science, Soochow University, Suzhou, Jiangsu, 215123, China

Keywords: N-isopropylacrylamide, stimuli-responsive microgels, monolayers, phase transition behavior, QCM-D.

**Abstract**

In this submission, the phase transition behavior for poly (*N*-isopropylacrylamide-co-acrylic acid) (pNIPAm-co-AAc) microgels and their assemblies was investigated as a function of temperature and pH using UV-Vis spectroscopy (to probe light scattering behavior) and quartz crystal microbalance with dissipation (QCM-D) measurements. PNIPAm-co-AAc microgels were "painted" onto Au-coated glass substrates (for UV-Vis) and the Au electrode of a QCM crystal to generate monolayers. The subsequent deposition of another Au layer on top of the pNIPAm-co-AAc microgel layer yields what is known as an etalon. UV-Vis/QCM-D measurements revealed that the temperature and pH responsivities for the microgel assemblies match well with their solution behavior. UV-Vis spectroscopy shows that the transmittance of the microgel monolayers decreased with increasing solution temperature at pH 3.0. At pH 6.5, the AAc groups in the microgels were deprotonated, leading to strong Coulombic repulsive forces inside the microgels that prevented their collapse and leads to minimal change in the transmitted light intensity. However, QCM-D analysis reveals more complex behavior as it is sensitive to the viscosity/viscoelasticity and thickness changes of the microgel layer, which ultimately depends on the microgels chemical composition and the interaction of the etalon's Au layer with the crystal. The maximum sensitivity to temperature is $0.8\times10^{-3}$ $^{o}C\cdot Hz^{-1}$, which is the most sensitive pNIPAm microgel-based QCM temperature sensor thus far reported in the literature. Finally, we exploit this new understanding to characterize the pH and ionic strength of a solution using pNIPAm-co-XAAc microgel-based etalon coated crystals. The research results and the sensing demonstration can inspire new and improved sensor designs for a

variety of analytes.

## 1. Introduction

"Smart" polymers have been extensively studied over the years due to their ability to switch their physical/chemical characteristics in response to external stimuli. Of these, poly (*N*-isopropylacrylamide) (pNIPAm) is a well-known thermoresponsive polymer that undergoes a transition from swollen (hydrophilic) to deswollen (hydrophobic) upon heating above pNIPAm's lower critical solution temperature (LCST) of ~ 32 $^{o}$C. Heating pNIPAm above its LCST perturbs its interaction with water, and leads to its transition to a relatively hydrophobic and collapsed state. It is worth noting that this hydrophilic-hydrophobic phase transition behavior is fully reversible over many cycles. PNIPAm's thermoresponsivity has been exploited for a wide variety of applications, e.g., as coatings,[1-2] as a carrier for therapeutic agents,[3] for photonic materials,[4-5] and other applications.[6-8]

Single pNIPAm chains can be crosslinked into a three-dimensional polymer networks that swell with water to form hydrogels and hydrogel particles (microgels). PNIPAm-based microgels, which exhibit hydrodynamic radii in range of ~100 nm to several microns, are capable of responding to temperature rapidly and reversibly, similar to their non-crosslinked counterparts.[9-11] That is, the microgels are hydrated and swollen with water at T < LCST, and undergo a sharp phase transition above the LCST to a relatively dehydrated/deswollen state. One approach to render pNIPAm-based microgels responsive to other stimuli is to copolymerize functional comonomers into the microgels at the time of synthesis. For instance, the introduction of acrylic acid (AAc) into the pNIPAm-based microgels renders them

responsive to pH.[12] This is due to the deprotonation (and ionization) of the weak acid when the solution pH > $pK_a$, causing the network to swell; the network deswells when the AAc is protonated at pH < $pK_a$.

In 2010, the Serpe Group reported on a pNIPAm microgel-based gold hybrid assembly, which exhibits visual color that can be changed upon application of external stimuli.[5] As shown in Scheme 1, such pNIPAm-based microgel assemblies are constructed by sandwiching a pNIPAm-based microgel monolayer between two thin gold layers. This structure is referred to as a Fabry–Pérot etalon (*or* etalon). When light impinges on the device, it resonates in the microgel-based cavity, resulting in light interference and visual color. The optical properties of the etalon can be monitored by reflectance spectroscopy and described by the equation:

$$m\lambda = 2ndcos\theta \quad (1)$$

where $m$ is the peak order, $n$ is the refractive index of the dielectric, $d$ is the spacing between the mirrors, and $\theta$ is the angle of incidence (~ $0^o$ in our experiments).[5]

When the microgels change diameter in response to stimuli, the thickness of the microgel monolayer ($d$) changes, yielding a change in the optical properties of the devices (i.e., $\lambda$), and a visual color change. We point out that the refractive index of the microgel layer also changes, but the optical properties are dominated by the microgel layer thickness. In order to gain a better understanding of the phase transition behavior (i.e., volume phase transition and/or solvation state) for pNIPAm-based microgels, we probe the light scattering (UV-Vis) and mechanical properties (quartz crystal microbalance with dissipation (QCM-D)) of the microgel layers and etalons.

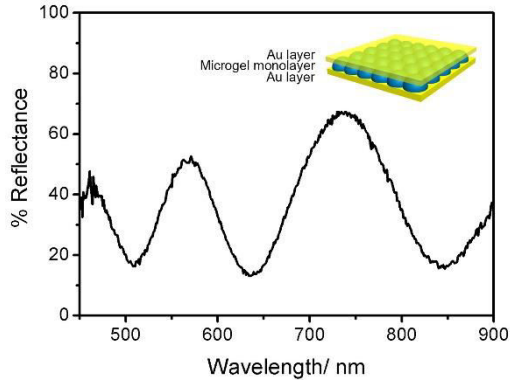


Scheme 1. A representative reflectance spectrum for a pNIPAm microgel-based etalon (inset: schematic structure of the etalon)

To date, the phase transition behavior for pNIPAm-based microgels has been investigated using a number of techniques, including turbidity measurements, thermal analysis, laser light scattering, and many other approaches.[13-18] However, there have been relatively few studies of the phase transition behavior of pNIPAm-based microgel assemblies relative to the number of studies of microgels dispersed in solution.[19-27] Quartz crystal microbalances (QCM) have been shown to be a powerful tool for investigating the properties of polymer thin films.[28-32] Although, in one example from the Lyon group, the phase transition behavior of pNIPAm-based microgel thin films in response to solution pH was investigated using a quartz crystal microbalance (QCM), surface plasmon resonance (SPR) and atomic force microscopy (AFM).[19] They found that pNIPAm-co-AAc microgel thin films responded to changes in pH, similar to the dispersed microgels in solution. However, the deposition of poly(allylamine hydrochloride) (PAH) on top of the microgel thin film significantly influenced the pH responsivity of the microgels, as evidenced by the QCM data. The data suggested that pH

responsivity depended on both the microgels' swelling and the interactions between the microgels and PAH. In another example, the Serpe group used QCM measurements to probe the response of pNIPAm-co-AAc microgel-based etalons to changes in solution temperature and pH. Although, this was in the context of quantifying the etalon response to generate sensors, and not focused on understanding the mechanical properties of the etalons and how they depend on solution temperature, pH, and microgel composition.[21]

In this submission, a series of pNIPAm-co-AAc microgels were synthesized with various AAc compositions. Monolayers of the microgels were assembled on surfaces (both Au-coated glass substrates and the Au electrode of a QCM crystal), and their response to solution temperature and pH evaluated using UV-Vis spectroscopy and QCM-D, respectively. Importantly, the response of pNIPAm-co-AAc microgel-based etalons to solution pH and temperature was studied by QCM-D. The data from the UV-Vis and QCM-D measurements showed that the temperature and pH responsivities were well retained once microgels were packed as a monolayer on a Au surface or confined between the two Au layers of an etalon. The trends in the transmittance data from UV-Vis measurements changed monotonically as a function of solution temperature at pH 3.0 and 6.5. By contrast, complex responses were observed in the QCM-D data for the surface bound microgels as solution temperature and pH changed. We attributed the behavior to the chemical composition of the microgels and their viscosity, the addition of a Au overlayer on the microgels and the entrapped water in the microgel matrix. The maximum sensitivity to temperature was $0.8\times10^{-3}$ $^{o}C\cdot Hz^{-1}$, which is the most sensitive pNIPAm-based QCM sensor reported thus far. These findings provide a good platform for better temperature sensors. Furthermore, we showed that the pNIPAm-co-XAAc

microgel-based etalon coated crystals were capable of detecting the pH and ionic strength of a solution. More importantly, our group has reported on numerous other etalon-based sensors for various analytes, which can also benefit from the results here.[33-36] As such, further work will look to exploit these finding to develop sensors for a variety of analytes of interest.

## 2. Experimental

### Materials

*N*-isopropylacrylamide was obtained from TCI (Portland, Oregon) and purified by recrystallization from hexane (≥ 98.5 %, Sigma-Aldrich) prior to use. N, N'-methylenebisacrylamide (BIS, 99 %), acrylic acid (AAc, 99 %) and ammonium persulfate (APS, 98 %) were purchased from Sigma-Aldrich (Oakville, Ontario). Sodium hydroxide was obtained from Anachemia Canada Inc (Mississauga, Ontario), and hydrochloric acid was purchased from Caledon Laboratories Ltd (Georgetown, Ontario). Disodium hydrogen phosphate dodecahydrate ($Na_2HPO_4$, ≥ 99 %), citric acid (≥ 99.8 %) and sodium chloride (NaCl, ≥ 99.8 %) were purchased from Sinopharm Chemical (China). These chemicals were used as received. Glass substrates (25 mm × 25 mm) were provided by Fisher (Ottawa, Ontario). Deionized (DI) water was filtered to have a resistivity of 18.2 MΩ·cm and was produced by a Milli-Q Plus system (Millipore Co.). Au (99.99%) and Cr (99.999%) were purchased from MRCS Canada (Edmonton) and ESPI (Ashland, OR), respectively.

### Microgel synthesis

A solution of NIPAm (11.9 mmol) and BIS (0.703 mmol) in 99 mL DI water was filtered

through a 0.2 µm filter, and subsequently added to a 250 mL 3-necked round bottom flask, which was fitted with a reflux condenser, nitrogen inlet, and temperature probe. The solution was purged with $N_2$ gas and heated to 70 °C for ~1 h. Next, AAc (1.43 mmol) was added to the heated reaction mixture. The reaction was then initiated with a solution of APS (0.2 mmol) in 1 mL of DI water. The reaction proceeded at 70 $^{o}$C for 4 h under $N_2$ gas. The resulting suspension was allowed to cool overnight, and then it was filtered through a Whatman #1 paper filter to remove any large aggregates. The microgel solution was then distributed into individual centrifuge tubes and purified *via* centrifugation at ~8300 rcf to form a pellet, followed by removal of the supernatant and resuspension with DI water, 6x. Microgels with varying AAc composition were synthesized in the same manner by keeping the total monomer concentration the same and varying the percent NIPAm in the reaction to accommodate the added AAc amount. In this paper, the microgels are referred to as pNIPAm-co-*X*AAc, where *X* represents the varying AAc concentration (X= 0%, 5%, 10% and 15%).

**"Large" diameter microgel synthesis**

The microgels were synthesized according to a previously published procedure.[37] A solution of NIPAm (17.0 mmol) and BIS (1.00 mmol) in 99 mL DI water was filtered through a 0.2 µm filter, and subsequently, added to a 100 mL 3-necked round bottom flask, which was fitted with a reflux condenser, nitrogen inlet, and temperature probe. The flask was heated to 45 °C in $N_2$ gas atmosphere for 1.5 h. Then, AAc (2.00 mmol) was added to the heated reaction mixture. The reaction was then initiated by addition of a 0.078 M aqueous solution of APS in 5 mL of DI water. After initiation, the reaction solution was heated to 65 °C at a rate

of 30 °C·h$^{-1}$ and the reaction proceeded overnight. The resulting suspension was allowed to cool overnight, and then it was filtered through a plug of glass wool to remove any coagulum. The microgel solution was then distributed into individual centrifuge tubes and purified *via* centrifugation at ~8300 rcf to form a pellet, followed by removal of the supernatant and resuspension with deionized water, 6x.

**Formation of microgel monolayers on glass**

A clean 25 mm × 25 mm glass substrate was coated with a thin layer of Cr (2 nm) and subsequently, a thin layer of Au (15 nm), using a thermal evaporation system (Torr International Inc.). Then the slides were annealed at 250 °C for 3 h. Next, they were cut to a size of 25 mm × 12.5 mm to fit into a cuvette for UV-Vis measurements. A microgel monolayer was assembled on the Au-coated glass using our previously reported "painting" protocol.[38] In brief, approximately 20 μL of concentrated pNIPAm-co-AAc microgels was spread on the Au/Cr (*or* simply Au)-coated glass substrate. The solution was allowed to dry completely over 2 h at 35 °C. The surface was then rinsed copiously with DI water to remove excess microgels not bound directly to the Au, and immersed in DI water at 30 °C overnight, prior to use.

**Formation of microgel monolayers and etalons on QCM crystals**

To form microgel monolayers on QCM crystals, the painting protocol detailed above was also used. Briefly, 12.5 μL of a concentrated, viscous microgel solution was painted on the "large" Au electrode of a cleaned QCM crystal (Q-Sense, Sweden, AT cut, 5 MHz, 14 mm

diameter).[29] After a homogeneous microgel monolayer was assembled on the electrode, a thin Cr and Au layer were deposited on the microgel layer via a thermal evaporation system, with a thickness of 2 nm and 15 nm, respectively. Finally, the microgel-based etalon coated QCM crystal was immersed in DI water at 30 °C overnight, prior to use.

**Characterization**

Attenuated total internal reflectance Fourier transform infrared spectroscopy (ATR-FTIR) spectra of lyophilized microgels were recorded on a Nicolet iS50 ATR FTIR spectrometer (Thermo Fisher Scientific, USA) in the range of 4000 – 500 $cm^{-1}$. The morphology and hydrodynamic diameter of the microgels was determined by transmission electron microscopy (TEM, Tecnai G2 spirit BioTwin, FEI, Co.,) and dynamic light scattering (DLS, Malvern ZS90, Scattering angle = 90°, 25 °C). For TEM, 100 μL of a highly concentrated microgel solution was dispersed in 45 mL of pH 3.0 solution. Approximately 5 μL of this dilute solution was deposited onto a Cu TEM grid and dried at room temperature. For DLS measurements, ~ 2 mL of the dilute solution was analyzed. The thickness of the microgel monolayer was measured using a Nanoscope V atomic force microscope (AFM, Bruker, U.S.). UV-Vis absorbance spectra were obtained by Hewlett Packard 8452A diode array spectrophotometer (Agilent Technologies, Inc., Santa Clara, CA). UV-Vis spectroscopy was used to determine the ability of the microgels to scatter light; the absorbance measured is directly proportional to the light scattering intensity, which can be related to the solvation state of the microgels. To conduct the measurements, a small amount of highly concentrated pNIPAm-co-*X*AAc microgels was diluted in DI water until the solution was visibly

transparent, and the solution pH adjusted to 3.0 by addition of HCl and 6.5 by addition of NaOH, respectively. UV-Vis spectra were recorded until the signal was stable at the given conditions. The absorbance (and related transmittance) value at 400 nm was used to report on the solvation state of the microgels suspended in solution and the microgel thin films in solution. That is, as the microgels collapse, they scatter more light, and the solution transmittance decreases. QCM-D measurements were performed with a Q-Sense-E4 instrument (Q-Sense, Sweden). QCM-D substrates were placed in the instrument's fluid chambers, and the experiments conducted in flow-through mode at a solution flow rate of 10 $\mu L \cdot min^{-1}$. For every experiment, the microgel-coated crystal was first incubated in a specific pH solution overnight, to ensure the microgel layer was completely swollen and stable. After that, it was incubated in the fluid chamber for ~ 50 min at 25 °C until stable QCM-D signals were obtained. The temperature of the pH solution in the chamber was increased from 25 to 45 °C at a rate of 0.333 °C $min^{-1}$ using a temperature controller. The shift in resonant frequency ($\Delta f_n$) and dissipation ($\Delta D$) at a series of overtones ($n$) and solution temperatures were collected as a function of time. The Sauerbrey equation is typically utilized to interpret QCM data. In this case, $\Delta f$ is proportional to the change in the adsorbed mass, as shown in equation 2.

$$\Delta f = -n\Delta m/C \qquad (2)$$

where $\Delta m$ is the adsorbed mass, n is the overtone number (1, 3, 5, 7, etc.) and C is a constant equal to 17.7 $ng \cdot Hz^{-1} \cdot cm^{-2}$ for the crystal.

The third overtone ($n$ = 3, ~ 15 MHz) was selected due to its relatively good signal-to-noise, and $\Delta f_3$ was simply referred to as $\Delta f$. The energy loss ($E_{lost}$) per stored energy ($E_{stored}$) during

one oscillation cycle is referred to as energy dissipation (*D*), as shown in equation 3.

$$D = E_{lost}/2\pi E_{stored} \qquad (3)$$

## 3. Results and discussion

PNIPAm-co-*X*AAc microgels were synthesized, and their chemical composition determined by ATR FTIR. As shown in Figure 1a, absorbance peaks centered at 1530 and 1650 $cm^{-1}$ can be ascribed to the N–H (amide II bond) and C=O (amide I bond) of NIPAm, respectively. As can be seen, as the amount of AAc incorporated into the microgel network increased, so did the intensity of the carboxyl stretching bands located at 1720 $cm^{-1}$. XPS was also used to confirm the chemical composition of the resultant pNIPAm-co-*X*AAc microgels. As can be seen in the XPS data in Figure 1b, $C_{1s}$, $N_{1s}$, $O_{1s}$ signals occur at 285.2, 399.2, 531.2 eV, respectively, in all samples. As *X* increases, the ratio of the intensity of $O_{1s}$ and $N_{1s}$ ($I_{O1s}/I_{N1s}$) increases from 0.16 to 0.20, which is an indicator of more AAc incorporated into the microgel (Figure S1, S2).

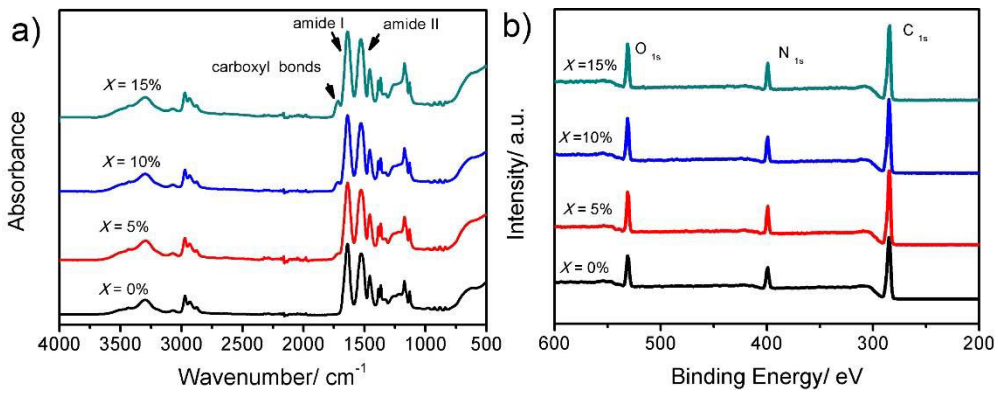


Figure 1. (a) ATR FTIR and (b) XPS spectra of pNIPAm-co-*X*AAc microgels.

Dynamic light scattering (DLS) was used to determine the average hydrodynamic diameter ($D_H$) of the microgels in solution at pH 3.0. Figure 2 shows that pNIPAm-co-0%AAc microgels exhibit the largest $D_H$ of 1060 ± 140 nm at pH 3.0, followed by pNIPAm-co-10%AAc microgels ($D_H$ = 780 ± 20 nm). However, pNIPAm-co-5%AAc and pNIPAm-co-15%AAc microgels exhibit a much smaller $D_H$ of 675 ± 6 and 685 ± 15 nm, respectively. Such a trend in $D_H$ with varying AAc composition in the microgels was supported by transmission electron microscope images (TEM, Figure S3). The pNIPAm-co-*X*AAc microgels in this submission were generated *via* homogenous nucleation at a temperature > the pNIPAm's LCST. Without the introduction of AAc monomer, pNIPAm particles tend to aggregate with others more readily *via* intermolecular H-bonding interactions, thus producing the largest $D_H$ after polymerization, and thus in pH 3.0 solution. In the presence of AAc, the aggregation of pNIPAm-co-*X*AAc is hindered possibly due to strong intramolecular H-bonding between NIPAm and AAc. This should yield a decrease in $D_H$ for microgels with increased *X*. However, pNIPAm-co-*X*AAc (*X*= 10% and 15%) microgels are relatively more swollen than pNIPAm-co-5%AAc microgel, due to the Coulombic repulsive forces that are still present as confirmed by zeta (ζ) potential data at pH 3.0 (Figure S3). Given that pNIPAm-co-*X*AAc (*X*= 10% and 15%) microgels show comparable ζ potential at pH 3.0 (Figure S3), it is expected that pNIPAm-co-10%AAc microgels should exhibit larger $D_H$ at that pH. As expected, pNIPAm-co-*X*AAc (X=5%, 10% and 15%) microgels are highly swollen due to the Coulombic repulsion at pH 6.5 (Figure S3)

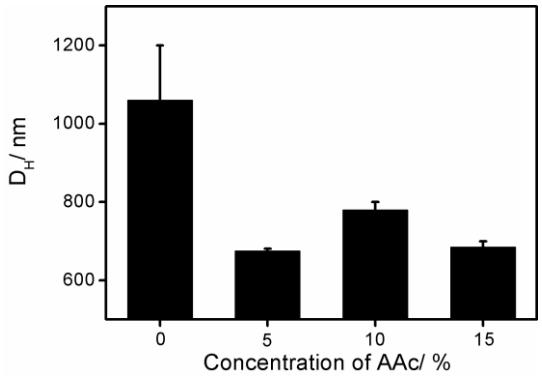


Figure 2. The hydrodynamic diameter ($D_H$) of pNIPAm-co-*X*AAc microgels at pH 3.0 measured by DLS.

Next, we investigated the phase transition behavior of pNIPAm-co-*X*AAc microgel dispersions at different solution pH, using UV-Vis spectroscopy to collect light scattering data. Again, when incident light passes through the microgel solution it is scattered, and the amount of scattered light can be related to the solvation state of the microgels. The data in Figure 3(a) shows that the transmittance decreased for microgels in pH 3.0 solution, when the temperature of the solution was increased from below to above pNIPAm's LCST. This is due to the collapse of the microgels, which increases their ability to scatter light. The data was fit by a sigmoidal curve with $R_{adj}^2 > 0.99$, then differentiated, and the temperature at the peak of the derivative curve is defined as the LCST. As shown in Figure 3, *X* has negligible effect on the value of the LCST for each sample at pH 3.0. At pH 6.5, a trend toward higher LCST with increasing *X* can be clearly seen in Figure 3(b). When the microgels were dispersed in pH 6.5 solution, the AAc groups were deprotonated. Consequently, the deswelling of the microgels is hindered due to the Coulombic repulsion between the AAc groups, which leads to the higher LCST with increasing *X*. Additionally, the LCSTs for the pNIPAm-co-10%AAc and

pNIPAm-co-15%AAc microgels cannot be observed over the temperature range investigated here. We also point out that the LCST of pNIPAm-co-0%AAc at both pHs are nearly identical. Therefore, it can be concluded from Figure 3 that the LCST for the given pNIPAm-co-*X*AAc microgels increases significantly when the pH of the solution was increased to above the $pK_a$ of AAc. It is also apparent that *X* significantly impacts phase transition behavior of pNIPAm-co-*X*AAc microgel dispersions at pH 6.5.

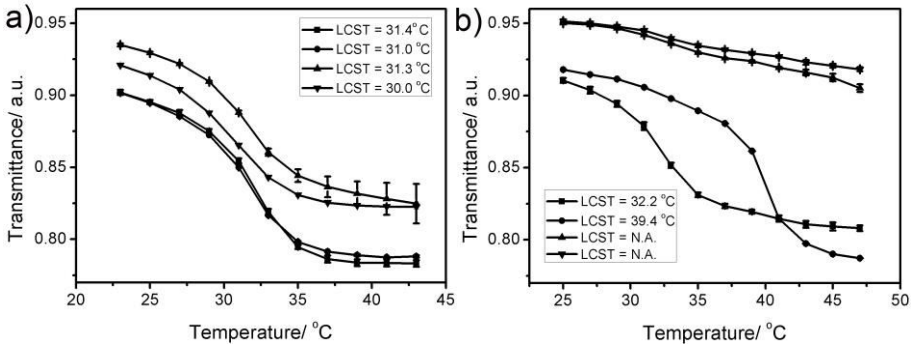


Figure 3. Changes in transmittance for pNIPAm-co-*X*AAc microgels as a function of temperature in (a) pH 3.0 and (b) pH 6.5 solution (*X* = (■) 0%, (●) 5%, (▲) 10%, (▼) 15%). Each data point in the average of 3 measurements, with the error bars showing the standard deviation.

We further studied the phase transition behavior for pNIPAm-co-*X*AAc microgel monolayers assembled on Au-coated glass surfaces (25 mm × 12.5 mm). Each sample was incubated in a cuvette containing a solution of a given pH, and the thermoresponsivity of the microgel monolayers investigated by UV-Vis. In this case, the light was passing through the glass slide normal to the surface, and is scattered in manner that can be related to the microgels solvation state. It is important to point out here that the Au layers were thin enough

to allow light to pass through to strike the microgels. From these experiments it can be seen that there is no apparent influence of *X* on the LCST at pH 3.0, whereas *X* has a significant influence on the phase transition behaviors for that at pH 6.5 (Figure 4). These experiments revealed that the microgel monolayers exhibit pH and temperature responsivity that is similar to the microgels dispersed in solution (Figure 3), and isn't dramatically affected by the microgel-microgel and microgel-Au interactions.[39]

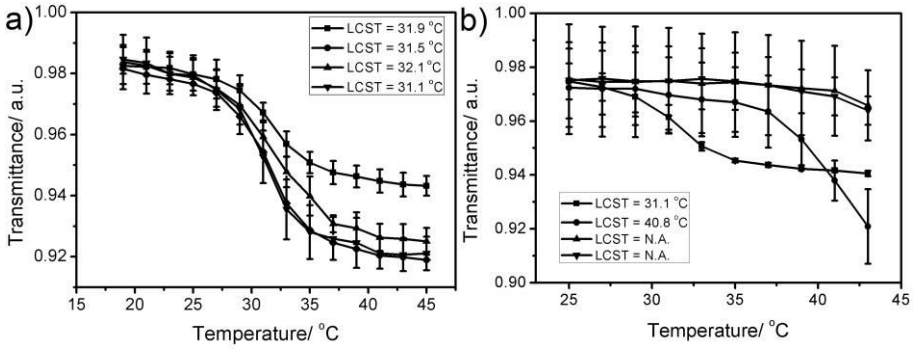


Figure 4. Changes in transmittance for pNIPAm-co-*X*AAc microgels as a function of temperature in (a) pH 3.0 and (b) pH 6.5 solution (*X*= (■) 0%, (●) 5%, (▲) 10%, (▼) 15%). Each data point in the average of 3 measurements, with the error bars showing the standard deviation.

Next, we investigated the thermo- and pH- responsivity of pNIPAm-co-*X*AAc microgel-based assemblies on the Au electrode of a QCM crystal (Figure 5(a)). The pNIPAm-co-*X*AAc microgel coated QCM crystals were incubated in the fluid chamber at a given pH for 50 min at 25 °C. The temperature of the pH solution in the chamber was increased from 25 to 45 °C over a 1 h period. Figure 5 shows the change in $\Delta f$ and $\Delta D$ for the bare quartz crystal in pH 3.0 solution at elevated temperature, which shows an increase in $\Delta f$

of ~100 Hz and a -25×$10^6$ change in $\Delta D$. This is likely a result of the decreased viscosity and density of the liquid upon heating. Herein, such solvent induced changes in QCM signals are referred to as $\Delta f$ (solvent) and $\Delta D$ (solvent), respectively. When the soft, water swellable pNIPAm-co-*X*AAc microgel monolayer was deposited on the crystal, the change of $\Delta f$ and $\Delta D$ became more complex (Figure 5(b-e)). To make our observations more clear, we divide the range of temperatures investigated into three stages. In the stage I, $\Delta f$ for the pNIPAm-co-0%AAc microgel coated QCM crystal dramatically decreased by -1790 Hz ($\Delta f_I$) when the temperature of pH 3.0 solution was increased from ~ 25 °C ($T_0$) to ~ LCST of the microgel ($T_1$ = 33.7 °C). In this stage we also observed that $\Delta D$ abruptly increased by 480×$10^{-6}$, suggesting more energy lost (dissipated) during one crystal oscillation cycle. Following the standard QCM theory, a large negative $\Delta f_I$ can be attributed to an increase in the mass and/or viscosity of the microgels on the QCM crystal as well as $\Delta f$ (solvent). When the temperature of the solution is increased to $T_1$, Figure 5(b) shows the value of $\Delta f$ (solvent) is -30 Hz, which appears negligible in comparison with the $\Delta f_I$ we detected. At pH 3.0, the microgels dehydrate and collapse at $T_1$ > LCST. This should yield a positive $\Delta f_I$ considering the mass loss of the water in the microgel matrix, as reported in the case of pNIPAm chains and microgels grafted to QCM surfaces.[24, 26] Also, dehydrated microgels become more rigid and should lead to a decrease in $\Delta D$. Therefore, the observed significantly reduced $\Delta f_I$ and increased $\Delta D_I$ was unexpected.

To explain this unexpected result, we further consider the thickness of the microgel monolayer. At $T_0$ and pH 3.0, pNIPAm-co-0%AAc microgels are swollen with a thickness of 290 ± 19 nm (measured by AFM, Figure S4), which is much thicker than the theoretical

penetration depth (δ) of the QCMs acoustic shear wave (~140 nm).[40] We point out that δ is the distance from the surface where the amplitude has decreased to 1/e times the amplitude at the sensor surface, which significantly impacts the sensitivity of the QCM crystal at δ. [41] Therefore, the QCM crystal cannot detect the mass of the solvated microgels accurately. Upon heating to $T_1$, the microgels collapse so that more "effective" mass of the microgels could be "felt" by the QCM crystal. We predict that this significant increase in "effective" mass results in the dramatic negative $\Delta f_I$ observed as the LCST is approached. As the microgels collapse, the dehydrated polymer chains in the microgels become more rigid. Simultaneously, as more "effective" mass of the microgels is "felt" by the QCM crystal, the acoustic shear wave will penetrate the dense microgel layer, yielding an increase in $E_{lost}$. This should dominate the observed large increase in the magnitude of $\Delta D_I$.

Immediately following stage I, the microgel layer continues to collapse as the temperature was increased from $T_1$ (33.7 °C) to $T_2$ (35.2 °C). $\Delta D_{II}$ was seen to steeply decrease by $180\times10^{-6}$, suggesting that microgel layer becomes less soft. This can be interpreted by the fact that the expelled water from the microgel matrix dominates the change in $\Delta D_{II}$. $\Delta f$ in stage II continued to decrease by ~ -1080 Hz ($\Delta f_{II}$), which is dominated by the increased viscosity of the microgel. As a result, we conclude that the large negative shift in stage I and II ($\Delta f_{I+II}$) is mainly caused by the increased viscosity of the microgels and, more importantly, the increased "effective" mass of the microgel felt by the QCM crystals due to microgels' collapse. When temperature exceeded $T_2$ (stage III), an increase in $\Delta f_{III}$ (~580 Hz) and a decrease in $\Delta D_{III}$ (~-285 $\times10^{-6}$ ) were observed. During the same stage, $\Delta f$ (solvent) increase by ~55 Hz and $\Delta D$ (solvent) decrease by $\sim15\times10^{-6}$ (Figure 5(b)). In this stage, the microgels

continue to collapse, further expelling water from the microgel matrix. Consequently, it can be predicted that $\Delta f_{III}$ is mainly dominated by the loss of entrapped water from the microgel. The dehydrated microgels become more rigid and lead to a decrease in $\Delta D_{III}$.

At pH 3.0, pNIPAm-co-*X*AAc microgels (X = 5, 10, 15%) exhibit thermoresponsivity, therefore pNIPAm-co-5%AAc and pNIPAm-co-10%AAc microgel coated QCM crystals exhibit trends in $\Delta f$ and $\Delta D$ that are similar to pNIPAm-co-0%AAc. These data can be seen in Figure 5(c, d). The reason for their behavior can be explained in the same manner as the pNIPAm-co-0%AAc layers above. Although, it is interesting to note that the stage I disappears in the case of pNIPAm-co-15%AAc microgel coated crystal (Figure 5e). After measuring the thickness of pNIPAm-co-*X*AAc microgel layer at pH 3.0 (Figure S4), we hypothesize that this unique difference is a result of the pNIPAm-co-15%AAc microgel layer being thinner than δ (123 ± 5 nm). Therefore, with increasing temperature, the decreased $\Delta f_{II}$ is mainly caused by the increased viscosity of the microgels. Compared with the data collected *via* UV-Vis spectroscopy, the complex features of the QCM-D data is mainly influenced by microgel composition (thus the resulting thickness of the layer) and viscosity of the microgel and water in the microgel network. Figure 5f shows that the value of $\Delta f_{I+II}$ strongly depends on the initial thickness of the microgel layer. Roughly, a thicker microgel monolayer is able to exhibit a larger negative shift in $\Delta f_{I+II}$. It should be noted that the Voigt model could not fit the experimental data well, suggesting that more fitting parameters need to be considered in addition to those already in the Voigt model. Although, this was not investigated further.

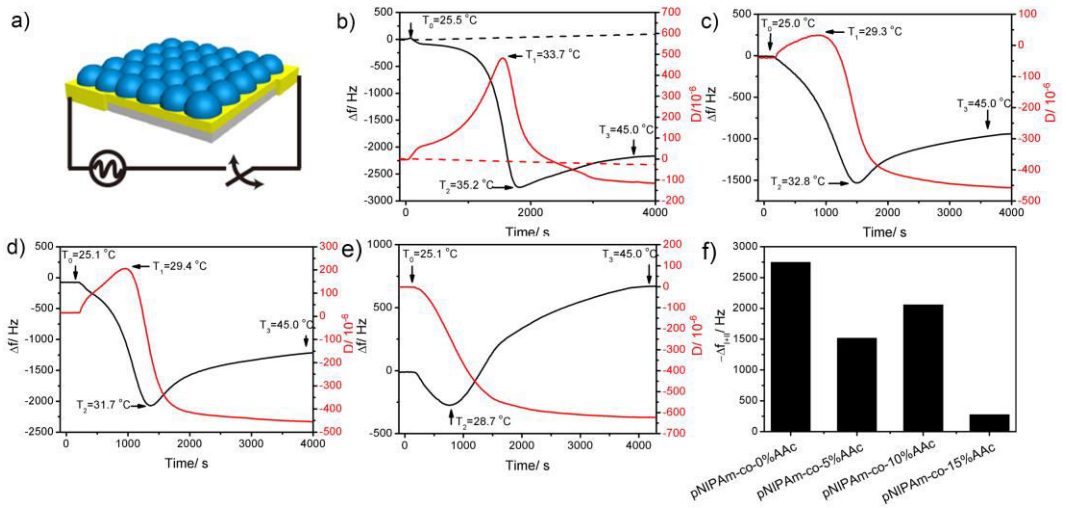


Figure 5. (a) Schematic representation of pNIPAm-co-*X*AAc microgel (blue spheres) coated on a QCM crystal (yellow) for QCM-D measurements. (b) (Black) frequency and (red) dissipation change for (b) the bare crystal (dashed) and pNIPAm-co-*X*AAc microgel coated crystal at pH 3.0, where *X* = (b, solid) 0%, (c) 5%, (d) 10% and (e) 15%. (f) The change in $\Delta f_{I+II}$ for pNIPAm-co-*X*AAc microgel coated crystal.

To test our hypothesis that the initial thickness of the microgel layer influences $\Delta f_{I+II}$, we further fabricated a microgel coated QCM crystal with "large diameter" pNIPAm-co-10%AAc microgels ($D_H$ = 1218 ± 180 nm, obtained by DLS, Figure S5, 6). Data shown in Figure S7 was obtained in the same manner as that in Figure 5. As predicted, the "large-diameter" microgels featured the three stages as mentioned above and the largest magnitude of $\Delta f_{I+II}$ (4620 Hz), presenting a sensitivity of $0.8\times10^{-3}$ $^{o}C\cdot Hz^{-1}$. This is the most sensitive pNIPAm-coated QCM crystal reported thus far (Table S1). Because the "large-diameter" microgel coated QCM crystal is highly swollen and yields the thickest film (>> δ), a majority of its may might not be detected at $T_0$ (25.5 $^{o}C$). Although, with an increase

in temperature to $T_2$ (35.3 $^{o}$C), the QCM crystal can detect an increment in the mass of the microgels, thus yielding the significant change of $\Delta f_{I+II}$.

Next, we studied the effect of temperature on the shift of $\Delta f$ and $\Delta D$ at pH 6.5 using the same samples as above (Figure 6). The bare crystals showed similar trends as that at pH 3.0 upon heating, featuring a ~100 Hz change in $\Delta f$ and a ~-30×10$^6$ change in $\Delta D$. In the absence of AAc, the observed changes in $\Delta f$ and $\Delta D$ for the pNIPAm-co-0%AAc microgel coated QCM crystal is the same as that at pH 3.0, where $\Delta f$ decreases by ~-2565 Hz and $\Delta D$ increases by ~390×10$^6$. Therefore, the explanation at the different stages of microgel deswelling should be the similar as above. The pNIPAm-co-5%AAc microgel coated QCM crystal shows that $\Delta f$ decreases before the temperature reaches 42.1 $^{o}$C ($T_2$), then increases by ~390 Hz. Simultaneously, $\Delta D$ decreases by ~-70 × 10$^6$ after reaching a maximum of ~210 × 10$^6$ at 39.5 $^{o}$C. The value of $T_1$ and $T_2$ shift towards much higher temperature than that at pH 3.0, indicating the LCST of PNIPAm-co-5%AAc microgel is increased at pH 6.5. This is unsurprising because the collapse of the microgel layer is hindered by the Coulombic repulsion inside of the microgels at high pH due to the deprotonation of the AAc groups. As discussed above, the highly swollen pNIPAm-co-5%AAc microgel layer produces a larger magnitude of $\Delta f_{I+II}$ at this pH. As long as the temperature is >> LCST, the microgels can deswell, giving rise to an increase in $\Delta f_{III}$. As the concentration of AAc in the microgels increases so does the magnitude of the Coulombic repulsion forces that prevent the microgels from collapsing at pH 6.5. Therefore, $T_1$ and $T_2$ shift to 43.8 and 45.0 $^{o}$C in the case of pNIPAm-co-10%AAc microgel coated crystal. Furthermore, $T_1$ and $T_2$ shift off the measurable range for pNIPAm-co-15%AAc microgel coated crystals at elevated temperature

and pH 6.5.

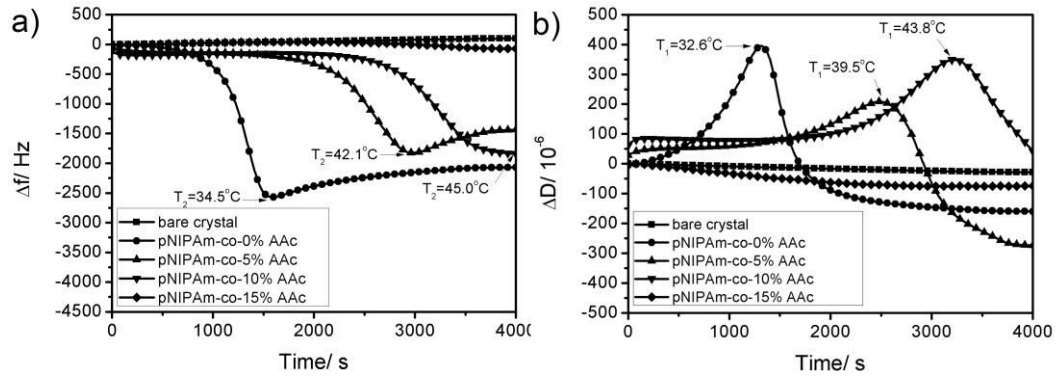


Figure 6. (a) Frequency and (b) dissipation change for (■) the bare crystal and pNIPAm-co-*X*AAc microgel coated crystal at pH 6.5, where the temperature of the solution was increased from $T_0$ (25.0 °C) to $T_3$ (45.0 °C). $T_1$ and $T_2$ for $X$ = 15% are not measurable on this scale.

In subsequent experiments, we fabricated a series of pNIPAm-co-*X*AAc microgel-based etalon coated QCM crystals. Similarly, thermo- and pH- responsivities of the pNIPAm-co-*X*AAc microgel assemblies were investigated using QCM-D at pH 3.0 and 6.5 (Figure 7, 8). The devices exhibited visible color, which was used to confirm its layered structure (Figure 7(a)). After the deposition of the Au overlayer on top of the microgel monolayer, we hypothesized that $\Delta f_{I+II}$ should be enhanced as the Au layer thickness increased. To evaluate this, experiments were performed in the same manner as those displayed in Figure 5. As shown in Figure 7, pNIPAm-co-*X*AAc microgel-based etalon (X= 5%, 10%, 15%) coated QCM crystals show very similar trends but enhanced magnitude of $\Delta f_{I+II}$ in comparison with the same devices without the deposited Au overlayer. For example, $\Delta f_{I+II}$ for pNIPAm-co-5%AAc microgel-based etalon coated QCM crystal decreased by ~ -3500 Hz,

whereas a change in ~-1500 Hz was observed for the QCM crystals coated with microgels without the addition of a Au layer on top. This enhanced response can be explained by the fact that the QCM crystal cannot truly detect the whole microgel matrix and thus cannot detect the mass of the Au overlayer at $T_0$ and pH 3.0 due to the thickness > δ. At $T_2$, the QCM crystal can detect more effective mass of the microgels and the Au layer due to the microgel collapse, leading to a larger negative shift in $\Delta f_{I+II}$. These results are consistent with our hypothesis that the change in $\Delta f_{I+II}$ depended dramatically on the thickness of the deposition layer. Unexpectedly, the change in $\Delta f_{I+II}$ for pNIPAm-co-0%AAc microgel-based etalon coated QCM crystal (~ -1000 Hz) is less than the counterpart without Au overlayer. A plausible hypothesis for the decreased $\Delta f_{I+II}$ in the case of pNIPAm-co-0%AAc microgel-based etalons is that the equilibrium swelling of microgels is hindered due to the relatively abundant :N-Au interactions between the pNIPAm-co-0%AAc microgels confined between the Au layers. These interactions are decreased for microgels with AAc as moles of NIPAm are replaced by AAc.

As a result, the pNIPAm-co-0%AAc microgel-based etalon coated QCM crystal shows a much lower thickness at $T_0$, yielding a decrease in $\Delta f_{I+II}$ in contrast to the microgel without Au overlayer, in 1 h.

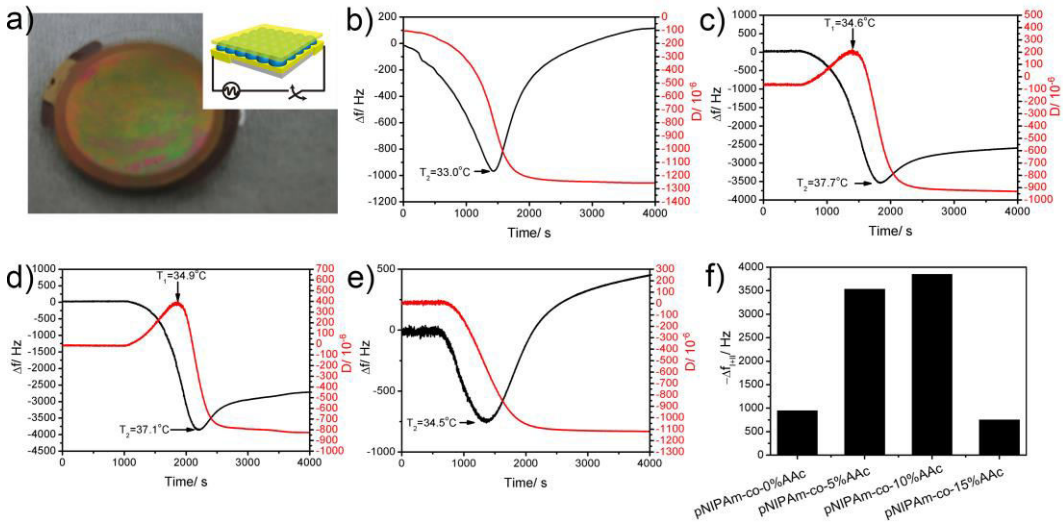


Figure 7. (a) A photograph of a typical pNIPAm-co-*X*AAc microgel-based etalon coated QCM crystal and (inset) its schematic representation. (Black) frequency and (red) dissipation change for pNIPAm-co-*X*AAc microgel-based etalon coated crystal at pH 3.0, where X = (b) 0%, (c) 5%, (d) 10% and (e) 15%. (f) The change in $\Delta f_{I+II}$ for pNIPAm-co-*X*AAc microgel-based etalon coated QCM crystal. Experiments were performed in the same manner as that displayed in Figure 5, where the temperature of the solution was increased from $T_0$ (25.0 °C) to $T_3$ (45.0 °C)

Finally, at pH 6.5, the changes in $\Delta f$ and $\Delta D$ in the case of pNIPAm-co-0%AAc microgel-based etalon coated QCM crystals are comparable to that at pH 3.0. In the case of pNIPAm-co-5%AA microgels, Coulombic repulsion results in an increase in $T_1$ and $T_2$ to 38.7 and 40.4 $^{o}$C, respectively. As mentioned above, the pNIPAm-co-5%AAc microgel-based etalon coated QCM crystal is highly swollen, therefore it yields a large magnitude of $\Delta f_{I+II}$ at pH 6.5. When temperature >> LCST, the microgels deswell, resulting in an increase in $\Delta f_{III}$. With increasing *X*, the stronger Coulombic repulsion forces prevent the microgel layer from

collapsing and therefore the value of $T_2$ shifts to a higher temperature. For instance, $T_1$ and $T_2$ cannot be observed in the case of pNIPAm-co-15%AAc microgel-based etalon coated QCM crystal.

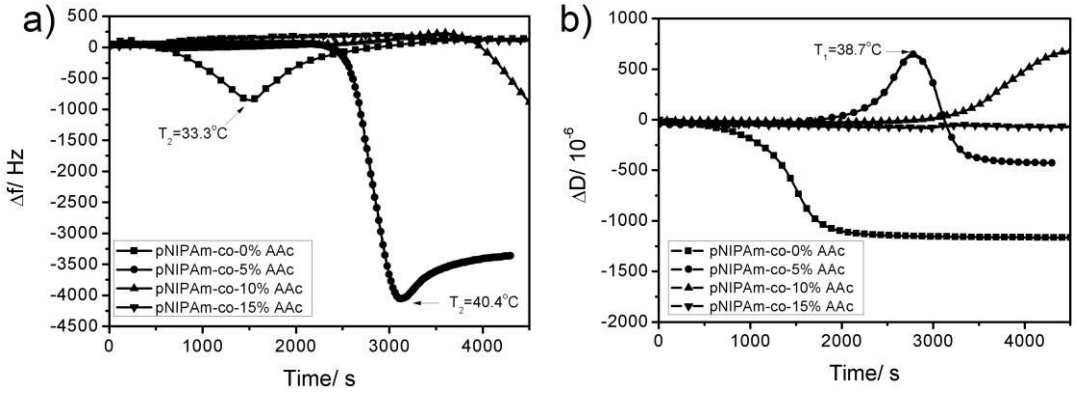


Figure 8. (a) Frequency and (b) dissipation change for pNIPAm-co-*X*AAc microgel-based etalon coated crystal at pH 6.5, where the temperature of the solution was increased from $T_0$ (25.0 °C) to $T_3$ (45.0 °C). $T_1$ for $X$ = 0% is not measurable on this scale; $T_1$ and $T_2$ for $X$ = 10% and 15% are not measureable on this scale.

To demonstrate the application of the systems investigated here, pNIPAm-co-*X*AAc microgel-based etalon coated crystals were shown to be capable of detecting the pH and ionic strength of a solution (Figure 9). Specifically, a pNIPAm-co-15%AAc microgel-based etalon coated crystal was incubated in $Na_2HPO_4$/citric acid buffer solution (pH = 7.33) at 25°C until its signal was stable. The pH of the solution was changed by varying the mole ratio of $Na_2HPO_4$ and citric acid, and Δf was recorded as a function of time. Figure 9(a) shows that Δf decreased with decreasing solution pH. Based on the results reported in this manuscript, we hypothesize that this is a result of more "effective" mass being felt by the QCM when the microgels dehydrate. The trend in −Δf as a function of pH is shown in Figure 9(b), which can

be fit with the equation shown in the inset with an $R_{adj}^2 > 0.99$. Additionally, Figure 9(c) shows that Δf decreases with increasing concentration of NaCl in solution (i.e., increasing ionic strength). In the absence of NaCl, the microgel monolayer is highly swollen in DI water at 25 $^{o}$C due to Coulombic repulsion of the deprotonated AAc groups in the microgels. As the concentration of NaCl increases, the microgels collapse due to charge shielding inside of the microgels. Again, more "effective" mass is being felt by the QCM crystal as the microgels collapse, which yields the observed decrease in Δf. As shown in Figure 9(d), Δf depends on the concentration of salt in solution and the equation in the figure inset can fit the data well. Therefore, our pNIPAm-co-*X*AAc microgel-based etalon coated crystals are able to detect the pH and ionic strength of the solution.

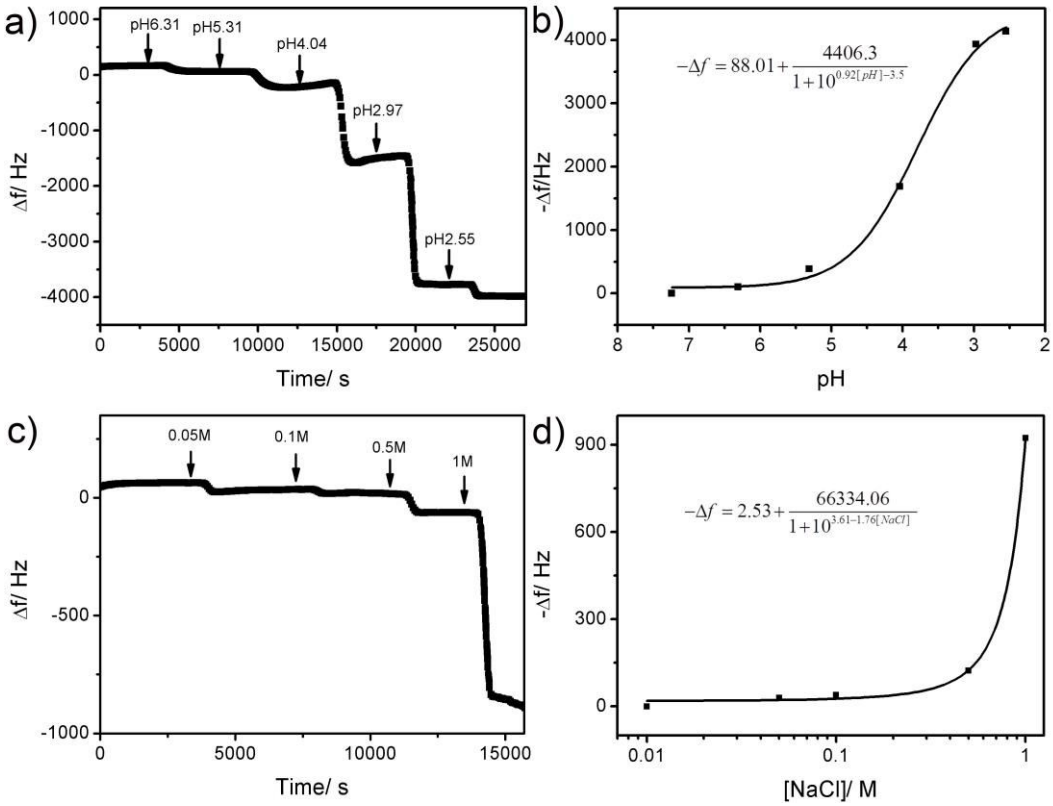


Figure 9. (a) Frequency change as a function of time as the solution pH was varied (indicated by the arrows above the data) and (b) the total frequency change at each pH for a

pNIPAm-co-15%AAc microgel-based etalon coated crystal at 25 °C. Also in (b) is a curve fit to the data (solid line) with the equation and fit parameters indicated in the inset. (c) Frequency change as a function of time as the solution ionic strength was varied (indicated by the arrows above the data) and (d) the total frequency change at each ionic strength for a pNIPAm-co-5%AAc microgel-based etalon coated crystal at 25 °C. Also in (d) is a curve fit to the data (solid line) with the equation and fit parameters indicated in the inset. We note that the flow rate was 10 μL $min^{-1}$, and due to this low flow rate, the devices appear to respond to solution pH and ionic strength changes slowly. As a result, the data in panels (a, c) are not representative of the true response kinetics of the devices.

## 4. Conclusions

In this paper, the phase transition behavior for pNIPAm-co-*X*AAc microgels and their assemblies was studied by UV-Vis spectroscopy and QCM-D. The results showed that the microgel monolayers and etalons were capable of responding to solution temperature and pH in a manner similar to the microgels dispersed in solution. The UV-Vis transmittance intensity of the microgel monolayers decreased the solution temperature was increased at pH 3.0, whereas it was hindered due to Coulombic repulsive forces at pH 6.5. In the case of pNIPAm-co-*X*AAc microgel assemblies coated on the Au electrode of a QCM crystal, we found that the change in $\Delta f$ and $\Delta D$ upon varying solution temperature and pH depended dramatically on the chemical composition (and thus hydrodynamic size) as well as the viscosity of the microgels, water in the microgel network and the Au overlayer. In specific, a large negative shift in $\Delta f_{I+II}$ is mainly caused by the increased viscosity of the microgels and,

more importantly, more "effective" mass felt by the QCM crystal due to microgel collapse. We hypothesize that $\Delta f_{III}$ was mainly due to the loss of mass by the expulsion of entrapped water. Dehydrated microgels become more rigid and lead to a decrease in $\Delta D_{III}$. The maximum sensitivity to temperature we detected was $0.8\times10^{-3}$ °C·Hz$^{-1}$. The pNIPAm-co-*X*AAc microgel-based etalon coated crystals were also shown to be capable of detecting changes in solution pH and ionic strength. This sensing capability can lead to more advanced sensor designs in the future.

## 5. Supporting Information

The XPS spectra and TEM of pNIPAm-co-*X*AAc microgels, Zeta potential data of pNIPAm-co-*X*AAc microgels at pH 3.0, AFM images of pNIPAm-co-XAAc microgel monolayer, dynamic light scattering and TEM for "large-sized" pNIPAm-co-10%AAc microgels at pH 3.0, DLS data of pNIPAm-co-XAAc microgels at 6.5, QCM-D signal change of "large-sized" pNIPAm-co-10%AAc microgels at pH 3.0 and elevated temperature, a survey on pNIPAm-based QCM chips upon temperature changes.

## 6. Author Information

Corresponding Author *E-mail: huliang@suda.edu.cn; michael.serpe@ualberta.ca.

### Notes

The authors declare no competing financial interest

## 7. Acknowledgements

MJS acknowledges funding from the University of Alberta (the Department of Chemistry and the Faculty of Science), the Natural Sciences and Engineering Research Council of Canada (NSERC), the Canada Foundation for Innovation (CFI), the Alberta Advanced Education & Technology Small Equipment Grants Program (AET/SEGP), Grand Challenges Canada and IC-IMPACTS. WX acknowledges Alberta Innovates Technology Futures for a Graduate Student Scholarship. LH thanks funding from the National Natural Science Foundation of China (51403231), the Priority Academic Program Development of Jiangsu Higher Education Institutions (PAPD) and the China Scholarship Council (CSC).

## 6. References

(1) Sun, T.; Wang, G.; Feng, L.; Liu, B.; Ma, Y.; Jiang, L.; Zhu, D. Reversible Switching between Superhydrophilicity and Superhydrophobicity. *Angew. Chem., Int. Edit.* **2004**, *43*, 357-360.

(2) Rotzetter, A. C. C.; Schumacher, C. M.; Bubenhofer, S. B.; Grass, R. N.; Gerber, L. C.; Zeltner, M.; Stark, W. J. Thermoresponsive Polymer Induced Sweating Surfaces as an Efficient Way to Passively Cool Buildings. *Adv. Mater.* **2012**, *24*, 5352-5356.

(3) Qiu, Y.; Park, K. Environment-Sensitive Hydrogels for Drug Delivery. *Adv. Drug Delivery Rev.* **2001**, *53*, 321-339.

(4) Karg, M.; Hellweg, T.; Mulvaney, P. Self-Assembly of Tunable Nanocrystal Superlattices Using Poly(NIPAM) Spacers. *Adv. Funct. Mater.* **2011**, *21*, 4668-4676.

(5) Sorrell, C. D.; Carter, M. C. D.; Serpe, M. J. Color Tunable Poly (N-isopropylacrylamide)-co-Acrylic Acid Microgel–Au Hybrid Assemblies. *Adv. Funct. Mater.*. **2011**, *21*, 425-433.

(6) Qiu, L.; Liu, D.; Wang, Y.; Cheng, C.; Zhou, K.; Ding, J.; Truong, V. T.; Li, D. Mechanically Robust, Electrically Conductive and Stimuli-Responsive Binary Network Hydrogels Enabled by Superelastic Graphene Aerogels. *Adv. Mater.* **2014**, 26, 3333-3337.

(7) Hu, L.; Sarker, A. K.; Islam, M. R.; Li, X.; Lu, Z.; Serpe, M. J. Poly (N-isopropylacrylamide) Microgel-Based Assemblies. *J. Polym. Sci., Part A: Polym. Chem.* **2013**, *51*, 3004-3020.

(8) Zhu, C. H.; Hai, Z. B.; Cui, C. H.; Li, H.-H.; Chen, J. F.; Yu, S. H. In Situ Controlled Synthesis of Thermosensitive Poly(N-isopropylacrylamide)/Au Nanocomposite Hydrogels by Gamma Radiation for Catalytic Application. *Small* **2012,** *8*, 930-936.

(9) Saunders, B. R.; Vincent, B. Microgel Particles as Model Colloids: Theory, Properties and Applications. *Adv. Colloid Interface Sci.***1999**, *80*, 1-25.

(10) Pelton, R. Temperature-Sensitive Aqueous Microgels. *Adv. Colloid Interfac.* **2000**, *85*, 1- 33.

(11) Karg, M.; Hellweg, T. New "Smart" Poly(NIPAM) Microgels and Nanoparticle Microgel Hybrids: Properties and Advances in Characterisation. *Curr. Opin. Colloid Interface Sci.* **2009**, *14*, 438-450.

(12) Kratz, K.; Hellweg, T.; Eimer, W. Influence of Charge Density on the Swelling of Colloidal Poly(N-isopropylacrylamide-co-acrylic acid) Microgels. *Colloids Surf., A* **2000**, *170*, 137-149.

(13) Daly, E.; Saunders, B. R. A Study of the Effect of Electrolyte on the Swelling and Stability of Poly(N-isopropylacrylamide) Microgel Dispersions. *Langmuir* **2000**, *16*, 5546-5552.

(14) Gan, D.; Lyon, L. A. Tunable Swelling Kinetics in Core−Shell Hydrogel Nanoparticles. *J. Am. Chem. Soc.* **2001**, *123*, 7511-7517.

(15) Cao, Z.; Du, B.; Chen, T.; Liu, H.; Xu, J.; Fan, Z. Fabrication and Properties of Thermosensitive Organic/Inorganic Hybrid Hydrogel Thin Films. *Langmuir* **2008**, *24*, 5543-5551.

(16) Hoare, T.; Pelton, R. Calorimetric Analysis of Thermal Phase Transitions in Functionalized Microgels. *J. Phys. Chem. B* **2007**, *111*, 1334-1342.

(17) Zhou, S.; Chu, B. Synthesis and Volume Phase Transition of Poly(methacrylic acid-co-N-isopropylacrylamide) Microgel Particles in Water. *J. Phys. Chem. B* **1998**, *102*, 1364-1371.

(18) Ahmed, Z.; Gooding, E. A.; Pimenov, K. V.; Wang, L.; Asher, S. A. UV Resonance Raman Determination of Molecular Mechanism of Poly(N-isopropylacrylamide) Volume Phase Transition. *J. Phys. Chem. B* **2009**, *113*, 4248-4256.

(19) Sorrell, C. D.; Lyon, L. A. Bimodal Swelling Responses in Microgel Thin Films. *J. Phys. Chem. B* **2007**, *111*, 4060-4066.

(20) Islam, M. R.; Johnson, K. C. C.; Serpe, M. J. Microgel-Based Etalon Coated Quartz Crystal Microbalances for Detecting Solution pH: The Effect of Au Overlayer Thickness. *Anal. Chim. Acta* **2013**, *792*, 110-114.

(21) Johnson, K. C. C.; Mendez, F.; Serpe, M. J. Detecting Solution pH Changes Using Poly(N-isopropylacrylamide)-co-acrylic acid Microgel-Based Etalon Modified Quartz Crystal Microbalances. *Anal. Chim. Acta* **2012**, *739*, 83-88.

(22) Wang, Z.; Kuckling, D.; Johannsmann, D. Temperature- Induced Swelling and De- swelling of Thin Poly(N- Isopropylacrylamide) Gels in Water: Combined Acoustic and Optical Measurements. *Soft Mater.* **2003**, *1*, 353-364.

(23) Plunkett, M. A.; Wang, Z.; Rutland, M. W.; Johannsmann, D. Adsorption of PNIPAM Layers on Hydrophobic Gold Surfaces, Measured in Situ by QCM and SPR. *Langmuir* **2003**, *19*, 6837-6844.

(24) Ishida, N.; Biggs, S. Effect of Grafting Density on Phase Transition Behavior for Poly(N-isopropylacryamide) Brushes in Aqueous Solutions Studied by AFM and QCM-D.

*Macromolecules* **2010**, *43*, 7269-7276.

(25) Alf, M. E.; Hatton, T. A.; Gleason, K. K. Novel N-isopropylacrylamide Based Polymer Architecture for Faster LCST Transition Kinetics. *Polymer* **2011**, *52*, 4429-4434.

(26) Ma, H.; Fu, L.; Li, W.; Zhang, Y.; Li, M. Real-Time Measurement of the Mass of Water Expelled by Poly(N-isopropylacrylamide) Brushes upon Thermo-Induced Collapse. *Chem. Commun.* **2009**, *23*, 3428-3430.

(27) Ishida, N.; Biggs, S. Salt-Induced Structural Behavior for Poly(N-isopropylacryamide) Grafted onto Solid Surface Observed Directly by AFM and QCM-D. *Macromolecules* **2007**, *40*, 9045-9052.

(28) Luan, Y.; Li, D.; Wang, Y.; Liu, X.; Brash, J. L.; Chen, H. $^{125}$I-Radiolabeling, Surface Plasmon Resonance, and Quartz Crystal Microbalance with Dissipation: Three Tools to Compare Protein Adsorption on Surfaces of Different Wettability. *Langmuir* **2014**, *30*, 1029-1035.

(29) Sigolaeva, L. V.; Gladyr, S. Y.; Gelissen, A. P. H.; Mergel, O.; Pergushov, D. V.; Kurochkin, I. N.; Plamper, F. A.; Richtering, W. Dual-Stimuli-Sensitive Microgels as a Tool for Stimulated Spongelike Adsorption of Biomaterials for Biosensor Applications. *Biomacromolecules* **2014**, *15*, 3735-3745.

(30) Park, E. J.; Draper, D. D.; Flynn, N. T. Adsorption and Thermoresponsive Behavior of Poly(N-isopropylacrylamide-co-N,N‘-cystaminebisacrylamide) Thin Films on Gold. *Langmuir* **2007**, *23*, 7083-7089.

(31) Vogt, B. D.; Lin, E. K.; Wu, W.-l.; White, C. C. Effect of Film Thickness on the Validity of the Sauerbrey Equation for Hydrated Polyelectrolyte Films. *J. Phys. Chem. B* **2004**, *108*, 12685-12690.

(32) Li, Z.; Xiang, Y.; Zhou, X.; Nie, J.; Peng, M.; Du, B. Thermo-Sensitive

Poly(DEGMMA-co-MEA) Microgels: Synthesis, Characterization and Interfacial Interaction with Adsorbed Protein Layer. *Chin. J. Polym. Sci.* **2015**, *33*, 1516-1526.

(33) Hu, L.; Serpe, M. J. Controlling the Response of Color Tunable Poly (N-isopropylacrylamide) Microgel-Based Etalons with Hysteresis. *Chem. Commun.* **2013**, *49*, 2649-2651.

(34) Zhang, Q. M., Berg, D., Duan, J., Mugo, S. M., Serpe, M. J. Optical Devices Constructed from Ferrocene-Modified Microgels for $H_2O_2$ Sensing. *ACS Appl. Mater. Interfaces.* **2016**, *8*, 27264-27269.

(35) Islam, M. R., Xie, S., Huang, D., Smyth, K., Serpe, M. J. Poly (N-isopropylacrylamide) Microgel-Based Optical Devices for Humidity Sensing. *Anal. Chim. Acta* **2015**, *898*, 101-108.

(36) Huang, H., Serpe, M. J. Poly (N- isopropylacrylamide) Microgel- Based Etalons for Determining the Concentration of Ethanol in Gasoline. *J. Appl. Polym. Sci.* **2015**, 132, 42106.

(37) Meng, Z.; Smith, M. H.; Lyon, L. A. Temperature-Programmed Synthesis of Micron-Sized Multi-Responsive Microgels. *Colloid Polym. Sci.* **2009**, *287*, 277-285.

(38) Sorrell, C. D.; Carter, M. C. D.; Serpe, M. J. A "Paint-On" Protocol for the Facile Assembly of Uniform Microgel Coatings for Color Tunable Etalon Fabrication. *ACS Appl. Mater. Interfaces.* **2011**, *3*, 1140-1147.

(39) Harmon, M. E.; Jakob, T. A. M.; Knoll, W.; Frank, C. W. A Surface Plasmon Resonance Study of Volume Phase Transitions in N-isopropylacrylamide Gel Films. *Macromolecules* **2002**, *35*, 5999-6004.

(40) Zhang, Y.; Du, B.; Chen, X.; Ma, H. Convergence of Dissipation and Impedance Analysis of Quartz Crystal Microbalance Studies. *Anal. Chem.* **2009**, *81*, 642-648.

(41) Ohlsson, G.; Langhammer, C.; Zorić, I.; Kasemo, B. A Nanocell for Quartz Crystal

Microbalance and Quartz Crystal Microbalance with Dissipation-Monitoring Sensing. *Rev. Sci. Instrum.* **2009**, *80*, 083905.

TOC image